JOURNAL OF MATERIALS SCIENCE 26 (1991) 43–48

Laser surface modification of a 13.5% Cr, 0.6% C steel

J. C. ION, T. MOISIO
Lappeenranta University of Technology Laser Processing Laboratory, SF-53851 Lappeenranta, Finland

T. F. PEDERSEN, B. SØRENSEN, C. M. HANSSON
The Danish Corrosion Centre, DK-2605 Brøndby, Denmark

A 13.5% Cr, 0.6% C steel, with an initial microstructure of chromium carbides in a ferrite matrix, was heat-treated by scanning a high-power laser beam over the surface. The aim was to compare the physical and chemical properties produced by this type of selective surface treatment with those resulting from a conventional furnace desensitization and quench-hardening heat treatment. Surface heating homogenized the carbon originally bound in the carbides sufficiently to produce martensite, giving hardening to levels comparable with a conventional heat treatment. Chromium-rich zones, carbides and retained austenite were also detected in the heated microstructure. Surface melting produced complete homogenization of both carbon and chromium, which resulted in the retention of large amounts of austenite in the microstructure on cooling to room temperature. Subsequent refrigeration at −196 °C transformed some of the austenite to martensite. Pitting corrosion and local reductions in hardness were observed adjacent to treated areas under certain conditions, due to precipitation of secondary carbides and elevated tempering, respectively.

1. Introduction

Multikilowatt industrial lasers provide a clean, localized, highly controllable heat source, which is ideal for general or selective treatment of engineering components. An area of considerable current interest is the modification of surfaces to fulfil particular corrosion and/or abrasion requirements, whilst retaining the good structural properties of the bulk, e.g. impact resistance. Such an approach provides many opportunities for component fabrication which lie outside the boundaries of traditional materials' selection criteria. The potential for savings in the use of costly and scarce alloying additions is great, and in addition, possibilities arise for the introduction of totally new manufacturing methods.

We have investigated the effects of rapid heating and cooling produced by laser surface treatment on the microstructure and properties of a commercially-available martensitic stainless steel, used in the production of cutting tools. This technique offers greater flexibility than conventional heat treatments, can be applied more selectively to a component, and may also prove to be more cost-effective. The material is normally delivered in a soft, annealed condition, suitable for forming, with a microstructure consisting of carbides in a ferrite matrix. In this state, the material is neither hard nor corrosion-resistant, because the principal alloying additions of chromium and carbon are bound in the carbides. The conventional heat treatment required for desensitizing involves austenitizing at around 1080 °C in a furnace or salt-bath in order to dissolve the carbides and homogenize the distribution of alloying elements. Subsequent quenching transforms austenite to martensite, producing a hard, corrosion-resistant component. For laser processing to be successful, the beam must be able to induce thermal cycles in surface regions of the material which are sufficient to dissolve the carbides, homogenize the relatively high concentrations of alloying elements, and produce martensite through self-quenching.

Surface heating [1] and melting [2], using a laser have been demonstrated as methods of desensitizing low-carbon austenitic stainless steels. Laser transformation hardening and glazing are proven methods of improving the surfaces of high carbon steels and cast irons [3, 4]. Laser hardening of chromium steel, initially in a conventionally heat-treated condition (a tempered martensite microstructure), has been performed with encouraging results [5, 6, 7]. However, work concerning the response of material originally in the as-delivered condition (hot rolled and annealed), is scarce.

2. Experimental procedure

2.1. Materials and processing

The steel, designated 12C27, was supplied by Suomen Sandvik OY. It was delivered as hot-rolled and annealed plate of thickness 4 mm. The composition is given in Table I. The microstructure consisted of $M_{23}C_6$-type carbides, between 1 and 10 μm diameter, in an equiaxed ferrite matrix. Samples with dimen-

0022–2461/91 $03.00 + .12

TABLE I Composition of the Sandvik 12C27 used (wt %)

C	Si	Mn	P	S	Cr	Ni	Mo	V	Ti
0.61	0.34	0.32	0.021	0.009	13.60	0.14	0.01	0.06	0.003

sions 260 mm × 75 mm were machined, suitable for laser treatment and the production of a variety of test pieces. Prior to treatment, the surface of the material was sandblasted, cleaned and sprayed with colloidal graphite in order to increase its absorptivity to the laser beam.

The laser, a fast axial flow design, was manufactured by Rofin Sinar Laser GmbH, and produced a raw 10.6 μm wavelength beam of diameter 35 mm, with a TEM_{20} mode and a continuous power output of up to 6 kW. The beam was formed into a 5 mm × 7 mm heating pattern of uniform power distribution using a water-cooled kaleidoscope. The beam power delivered to the workpiece, which is used throughout this paper, was calibrated using a black body absorption device.

Samples were clamped to a thermally conducting plate for processing. This provided an efficient heat sink, and helped to reduce distortion and the effects of bulk heating. The laser beam was scanned across the sample surface using a programmable numerically-controlled beam-delivery system. Velocities could be reproduced with an accuracy better than ± 1%, and the power stability during the course of a treatment was typically ± 2%. The treated area was shrouded with a stream of argon, coaxial with the beam, in order to minimize oxidation. The effects of parameter variations on the surface microstructure were investigated by making single scans, which produced tracks of width 5 or 7 mm. A number of larger treated areas were built up by overlapping adjacent scans by approximately 1.5 mm, in order to investigate the effects of multiple thermal cycles. Samples were normally allowed to cool to room temperature between scans, but in a number of cases advantage was taken of the preheating effect of a previous scan.

Some samples of the annealed material were heat-treated conventionally in a furnace, to provide a comparison. This comprised austenitizing at 1082 °C (± 3 °C) for 15 min, quenching to 20 °C in circulating oil, followed by tempering for 30 min at 350 °C. A protective coating was applied prior to treatment to reduce decarburization during austenitizing.

2.2. Metallurgical analysis

After treatment, the samples were sectioned, polished and prepared for metallurgical examination of both transverse and longitudinal sections. Some specimens were cooled in liquid nitrogen at − 196 °C for 3 h, to investigate the effects of refrigeration on the microstructure and properties. Transverse and longitudinal sections were prepared for optical metallography by etching in an aqueous solution of 30 wt % HNO_3. Hardness profiles were made with a diamond pyramid indentor using a load of 300 g for 15 sec.

The volume fraction of retained austenite was calculated by measuring the intensities of X-ray diffraction peaks from the austenite and martensite phases, from a 5 mm × 2 mm area on the surface, to a depth of approximately 10 μm. When corrected for their structure factors, these gave values for the volume fractions of the two phases. Residual stresses were determined by measuring the variation in the crystal lattice spacing as a function of plane orientation, using CrK_α and MnK_α radiation in the martensite and austenite phases, respectively. Scanning electron microscopy (SEM) was used to identify the surface microstructures and phase morphologies, and energy-dispersive X-ray analysis (EDX) used to determine chromium concentration profiles in the matrix.

The sensitivity to pitting corrosion of the lightly ground surfaces was investigated in artificial seawater. A 38 mm diameter area of the sample formed the base of a corrosion cell, in which there was also a stainless steel counter electrode and a saturated calomel reference electrode. The electrodes were coupled to a potentiostat and a cathodic potential of −850 mV SCE was applied to the sample for 1 h in order to reduce any surface films. The applied potential was then removed and the sample allowed to stabilize before the polarization test was begun. An anodic potential was applied in steps of 10 mV min^{-1} from the corrosion potential up to +700 mV. The current flowing between the sample and the counter electrode was recorded, and used to generate a "polarization curve". Macrographs were made of the surfaces after testing.

3. Results

3.1. Nature and geometry of the treated zone

Optical micrographs of transverse sections from typical melted and hardened zones are illustrated in Fig. 1. The etchant shows clearly the geometry of the melted region. Hardness profiles confirmed that the hardened zone was equally well revealed by the etchant. Shallow hardened zones were rectangular in section, rounded at the corners, mirroring the power distribution in the beam section. The zone became more elliptical/circular in shape with increasing depth, due to the effects of bulk heating. The geometry of the melted zones followed a similar progression. Throughout this paper surfaces which were hardened, but not melted, are referred to as heated surfaces.

3.2. Physical properties of heated surfaces

Vertical hardness profiles, made at the centre-line of transverse sections of hardened tracks, showed a continuous decrease from a maximum at the surface to a depth corresponding to a hardness of approximately 350 HV0.3. Thereafter the hardness rapidly decreased to that of the annealed base material (200 HV0.3). A typical hardness profile is shown in Fig. 2. A selec-

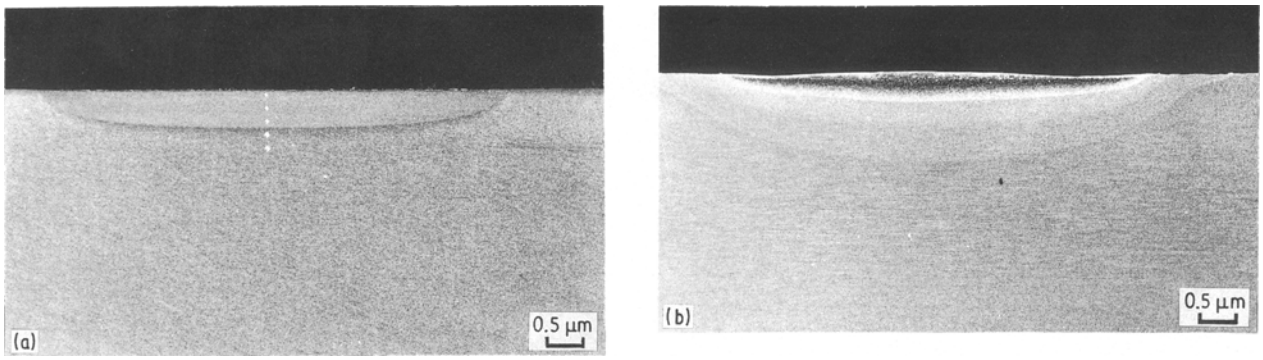

Figure 1 Transverse sections of laser-treated Sandvik 12C27 illustrating: (a) surface-hardened zone (including hardness indentations), (b) surface-melted and hardened zone. Etchant 30 wt % HNO_3.

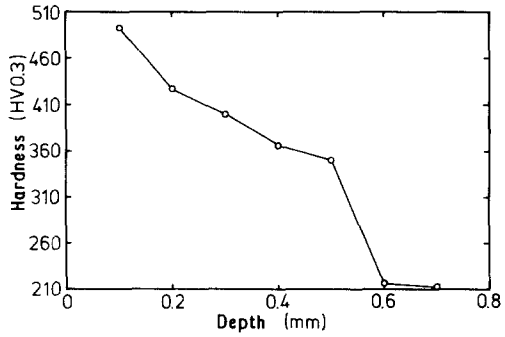

Figure 2 Vertical hardness profile taken at the centre of a laser-hardened track on Sandvik 12C27 (after cooling in liquid nitrogen). Power 2.1 kW, speed 700 mm min^{-1}, beam width 7 mm.

TABLE II Physical properties of a selection of regions heated using a uniformly distributed rectangular laser beam of width 7 mm and length 5 mm

Beam power (kW)	Beam velocity (mm min^{-1})	Maximum hardness (HV0.3)	350 HV0.3 depth (mm)	Retained austenite (vol %)
2.1	350	564	0.90	0
2.1	700	502	0.52	–
3.9	1500	618	0.72	48
3.9	2000	618	0.73	63
3.9	3000	662	0.44	68
4.5	1500	618	0.75	61
4.5	2500	511	0.54	69

tion of maximum hardness measurements taken from heated regions is given in Table II. The average maximum hardness was 585 HV0.3, which can be compared with 552 HV10 obtained by quenching furnace-austenitized material, and 505 HV1 following tempering. Little influence of processing parameters on the maximum hardness attained was evident, but the depth of hardening decreased rapidly with an increase in velocity. In regions adjacent to track overlaps, hardness reductions of approximately 100 HV0.3 were observed.

Significant amounts of retained austenite were detected in hardened regions, as shown in Table II. Refrigeration to −196 °C transformed some of the austenite to martensite, producing a slight increase in hardness. Compressive residual stresses of the order 750 and 550 MPa were detected in martensite and austenite, respectively.

EDX analysis revealed that chromium homogenization in the matrix of heated regions close to the surface, or beneath a melted zone, was extensive. In Fig. 3 it can be seen that the etchant attacks preferentially the matrix, which in the base material was ferrite, and in regions in which the A_{c1} temperature was exceeded, was martensite. Two types of lighter coloured regions are revealed. The brighter, spherical regions are carbides which survived the thermal cycle. The slightly darker, less distinct phase which appears to be continuous in regions close to the melt zone, is retained austenite.

3.3. Physical properties of melted surfaces

Regions which had been melted consisted primarily of retained austenite, with some martensite. The presence of the martensitic phase was revealed as a broadening of the X-ray diffraction peak (2 1 1). EDX analysis showed that chromium carbides were dissolved in the melt region, Fig. 4. The hardness of a melted region was approximately 390 HV0.3. Below the melted region, the hardness profile typically followed that of a heated surface. Refrigeration in liquid nitrogen raised the hardness of the melted region to approximately 650 HV0.3, but did not affect the properties of the underlying hardened region very significantly.

3.4. Corrosion properties of heated surfaces

Fig. 5a shows a laser-heated sample produced with a rapid processing speed after anodic polarization in artificial sea-water. Severe pitting, primarily adjacent to the edges of tracks is observed, together with general corrosion in the centres of the tracks and crevice corrosion around the circumference of the tested area (under the gasket of the cell). SEM revealed that much of the pitting attack took place at grain boundaries, and in the overlap regions where primary carbides had not been dissolved completely, or secondary precipitation had occurred, Fig. 6a. At the track centre, a less severe general type of attack was observed, Fig. 6b. Pitting potentials lay in the region −100 to

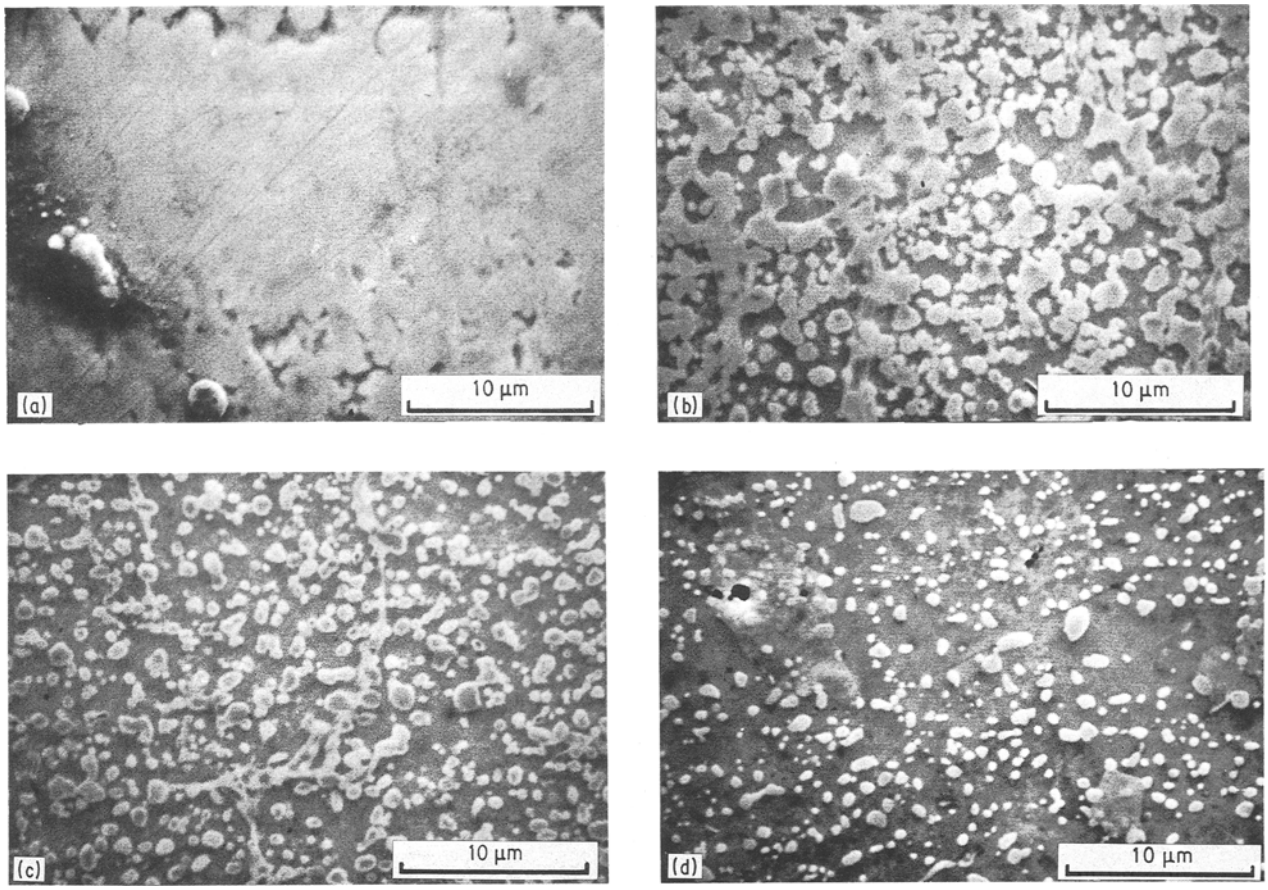

Figure 3 Secondary electron images taken from a laser-treated region of Sandvik 12C27, illustrating progressive dissolution of carbides (discrete particles) and formation of austenite (continuous light grey phase). (a) Melted surface layer, (b, c) hardened region below the melted zone, (d) base material. Etchant 30 wt % HNO_3.

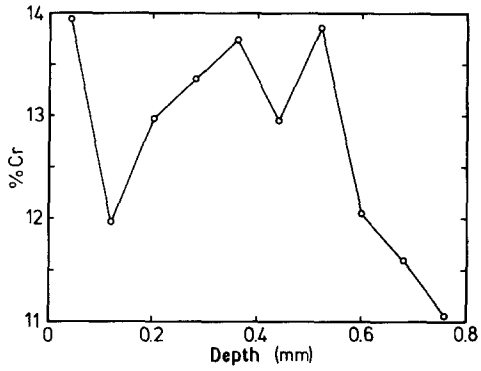

Figure 4 EDX chromium concentration profile in surface-melted region of Sandvik 12C27.

– 300 mV SCE, but were not always clearly defined on the polarization curves.

3.5. Corrosion properties of melted surfaces

Fig. 5b shows the surface of a laser-melted specimen, produced using a rapid travel speed with preheating, after corrosion testing. The individual melted tracks cannot be distinguished in this case, implying that the alloying elements have been homogenized in the surface. The surface topography after testing was such that it was difficult to determine if the corrosion attack was general or fine, uniformly distributed pitting at-

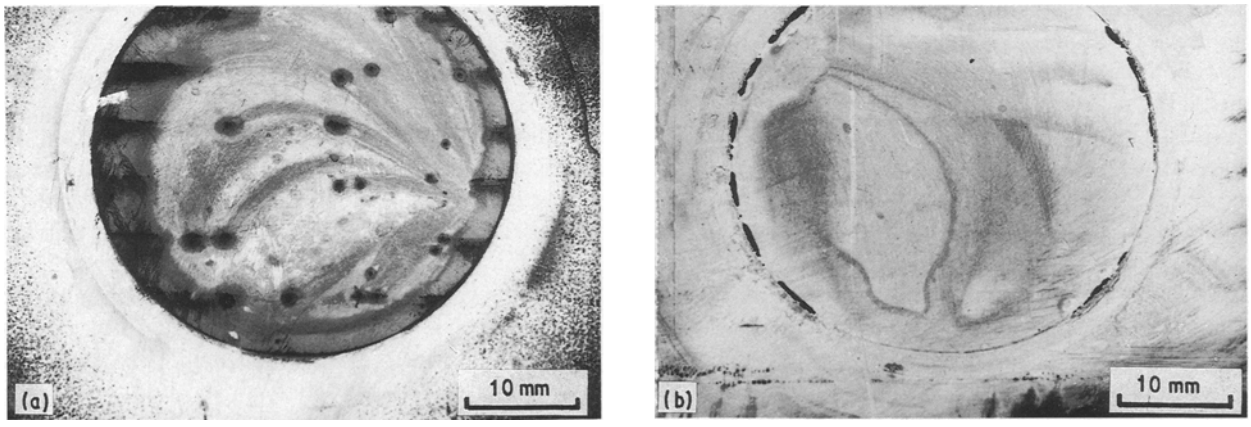

Figure 5 (a) Pitting corrosion primarily in the vicinity of the overlap regions of tracks in a laser-hardened sample. (b) Fine pitting attack uniformly distributed over the surface of a rapidly processed, laser-melted sample.

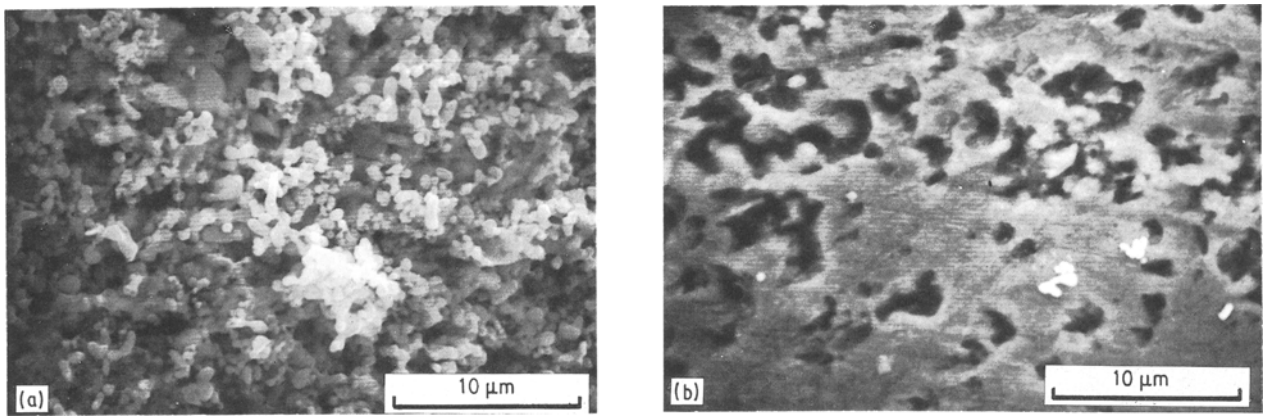

Figure 6 Secondary electron micrographs showing: (a) pitting corrosion in a hardened track overlap region, (b) general attack in the centre of a melted track.

tack. A pitting potential of −150 mV was recorded, possibly due to crevice corrosion observed under the gasket of the cell. In contrast, samples which were melted using low travel speeds exhibited general corrosion at the track overlaps, and pitting corrosion in adjacent regions, resulting in a more cathodic (inferior) pitting potential.

3.6. Corrosion properties of conventionally treated 12C27

Corrosion in the conventionally heat-treated samples occurred in the form of a few randomly distributed pits, combined with crevice corrosion under the gasket. The pitting potential was of the order −75 mV SCE.

4. Discussion

Dissolution of chromium carbides in regions in which the melting temperature is approached, significantly influences the microstructure on cooling. Diffusion of carbon in austenite occurs more rapidly than chromium; the activation energies are 142.4 and 231.9 kJ mol^{-1}, respectively [8]. Carbon homogenization appears to be complete in regions heated above the carbide dissolution temperature, with the result that martensitic transformation is possible on cooling, with the carbon increasing the martensite hardness considerably. However, the martensite start (M_s) and finish (M_f) temperatures are depressed by both chromium and carbon in solution in austenite [9]. Diffusion of chromium into the matrix surrounding the original carbides therefore depresses M_s locally, with the result that austenite is retained in these high concentration regions. The progress of this as a function of depth below the surface is illustrated in Fig. 3. The amounts of retained austenite detected using X-ray diffraction measurements correspond approximately with those observed in etched sections.

Regions which had been melted consisted almost entirely of retained austenite, due to element homogenization and depression of the M_s temperature throughout the melt zone. Under equilibrium conditions, ferrite is predicted to solidify initially from the melt, followed by austenitic transformation, and subsequent formation of ferrite and $M_{23}C_6$-type carbides [10]. Conditions pertaining to laser treatment are far from equilibrium, with cooling rates of the order 10 000 K sec^{-1}. Methods for assessing the weld metallurgy of stainless steels using chromium and nickel equivalents predict a fully austenitic solidification mode [11], and a fully austenitic room-temperature microstructure [12]. Techniques for taking rapid weld-pool solidification and solid-state cooling into account also predict a fully austenitic microstructure [13]. Rapid solidification of 0.5 wt % C, 10 wt % Cr steel following laser melting has been reported to produce a martensitic microstructure with M_3C carbides and retained austenite [14]. The results of this investigation appear to be consistent with conventional techniques of non-equilibrium microstructural prediction, although the exact nature of the carbides was not determined.

Carbides were found in overlap zones of both heated and melted tracks, where reheating had occurred. It was not possible to determine whether these were partially dissolved primary carbides, or secondary carbides precipitated during reheating. Reprecipitation of a variety of carbide types, depending on the tempering temperature, has been reported in this type of steel [9].

The theoretical hardness of martensite with a composition corresponding to the analysis is around 800 HV [15]. The shortfall in the maximum hardnesses measured in both heated and melted regions could be due to a number of factors: (i) incomplete carbon homogenization in austenite, or decarburization during treatment, both of which would result in martensite with a lower carbon content than the nominal; (ii) the retention of austenite on cooling; and (iii) the presence of austenite decomposition products other than martensite. The results show that the majority of the shortfall in both heated and melted surface hardnesses is due to the presence of retained austenite. The observation of retained austenite at −196 °C in melted and in a number of hardened regions, indicates that considerable homogenization of alloying elements can occur during laser heat treatment.

The degree of passivity and the pitting potential, E_p, are strongly dependent on the concentration of chromium in solution in the matrix, and decrease rapidly

when the level falls below 11.5 wt %. Thus, the higher values of E_p exhibited by the conventionally heat-treated samples relative to those of the laser-treated samples can probably be attributed to loss of chromium by evaporation during processing. Alternatively, or additionally, the higher carbon content of the laser-treated samples, resulting from diffusion and dissolution of the graphite absorption layer, could bind more of the chromium, thereby rendering the surface more susceptible to pitting.

For the laser-heated samples, the chromium content of the matrix at the centre of tracks of samples with low E_p indicates that during rapid processing, only limited homogenization of the chromium is achieved. The observation that pitting occurred preferentially in the vicinity of the overlap regions of the tracks is due to their lower chromium content, caused by a combination of insufficient primary carbide dissolution and secondary precipitation. This results in a galvanic effect between the overlap regions and the control regions of the centres of the tracks, with the control regions being effectively protected by the more anodic overlap regions.

The laser-melted samples processed at a high traverse rate did not exhibit any preferential pitting in, or adjacent to, the overlap regions. This suggests that the treatment was sufficient to dissolve the carbides, and the cooling rate was sufficient to prevent any re-precipitation. In contrast, the laser-melted samples processed at lower traverse rates exhibited preferential corrosion in the vicinity of the overlap region. This again may be due to either evaporation of chromium during the second melting, or to secondary carbide precipitation during cooling.

5. Conclusions

Laser surface heating of annealed Sandvik 12C27, without melting, can result in extensive dissolution of chromium carbides along the track centre-line, but limited dissolution towards the edges. Redistribution of carbon is sufficient to produce hardening by martensitic transformation, but the high alloy content results in depression of the martensite finish temperature and, consequently, the retention of austenite at room temperature. Hardness levels are comparable with those produced by a conventional heat treatment. Pitting corrosion attack in the track centres may occur if insufficient time for homogenization of the alloying elements is allowed, i.e. if processing speeds are too high.

Laser surface melting results in complete dissolution of the carbides and homogenization of the alloying elements. Surface hardnesses are relatively low due to the retention of large amounts of austenite on cooling to room temperature, but can be increased to levels associated with conventional heat treatments by refrigeration in liquid nitrogen. The corrosion characteristics are more uniform, with less pitting attack.

Pitting corrosion and local reductions in hardness may be observed adjacent to treated areas, particularly when the processing speed is low. Corrosion is caused by a combination of insufficient dissolution of primary carbides, precipitation of secondary carbides and evaporation of chromium. Softening is a result of tempering from adjacent treated regions.

Rapid laser treatments which produce surface peak temperatures close to the melting temperature, but which minimize the time available for reprecipitation and tempering, give rise to surfaces which possess physical and chemical properties comparable with conventional furnace heat treatments. The difficulty in producing hardening and corrosion resistance simultaneously in this type of highly alloyed steel, using a laser beam, indicates that a new philosophy in designing steel compositions is required, if full advantage is to be gained from the increasing availability of lasers in surface treatment.

Acknowledgements

The authors acknowledge helpful discussions with Erkki Veijalainen, and the assistance of Esko Reinikainen and Pertti Kokko with metallography and laser processing, respectively. Financial support was provided by the Nordic Fund for Technology and Industrial Development, the Danish Technical and Scientific Council, the Finnish Technology Development Centre (TEKES), Danfoss A/S and Bruel and Kjaer.

References

1. Y. NAKAO and K. NISHIMOTO, *Trans. Jpn Weld. Soc.* **17** (1986) 84.
2. T. R. ANTHONY and H. E. CLINE, *J. Appl. Phys.* **49** (1978), 1248.
3. H. W. BERGMANN, *Surface Engng* **1** (1985) 137.
4. P. A. MOLIAN, *ibid.* **2** (1986) 19.
5. J. KUSINSKI and G. THOMAS, in "Proceedings of the Conference on Laser Processing: Fundamentals, Applications, and Systems Engineering", edited by W. W. Duley (SPIE, Washington, 1986) pp. 150–6.
6. J. COM-NOUGUÉ and E. KERRAND, in "Proceedings of the Materials Processing Symposium ICALEO '84", Boston, edited by J. Mazumder (Laser Institute of America, Ohio, 1984) pp. 112–9.
7. M. ROTH and M. CANTELLO, in "Proceedings of the 2nd International Conference on Lasers in Manufacturing", Birmingham, edited by M. F. Kimmitt (IFS, Bedford, 1985) pp. 119–28.
8. S. MROWEC, in "Defects and Diffusion in Solids – An Introduction" (Elsevier, Amsterdam, 1980) pp. 400–14.
9. K. J. IRVINE, D. J. CROWE and F. B. PICKERING, *J. Iron Steel Inst.* **195** (1960) 386.
10. M. MANNERKOSKI, '*Acta Polytechnica Scandinavia*' no. 26 (Finnish Academy of Technical Sciences, Helsinki, 1964).
11. T. A. SIEWERT, C. N. McCOWAN and D. L. OLSON, *Weld. J.* **67** (1988) 289-s.
12. A. L. SCHAEFFLER, *Met. Prog.* **56** (1949) 680.
13. S. A. DAVID, J. M. VITEK and T. L. HEBBLE, *Weld. J.* **66** (1987) 289-s.
14. P. A. MOLIAN and W. E. WOOD, *Mater. Sci. Engng* **62** (1984) 271.
15. G. KRAUSS, in "Hardenability Concepts with Applications to Steel", edited by D. V. Doane and J. S. Kirkaldy (AIME, Warrendale, 1978) pp. 229–48.

Received 14 August 1989
and accepted 1 February 1990